Draft version March 8, 2001
Preprint typeset using LaTeX style emulateapj

GASEOUS SUBSTRUCTURE IN TIDAL TAILS AND THE FORMATION OF TIDAL DWARF GALAXIES

J. E. Hibbard
National Radio Astronomy Observatory[1], 520 Edgemont Road, Charlottesville, VA, 22903;
(*jhibbard@nrao.edu*)
AND
J. E. Barnes
Institute for Astronomy , University of Hawaii, Honolulu, HI, 96822; (*barnes@ifa.hawaii.edu*)
AND
J. M. van der Hulst
Kapteyn Astronomical Institute, Postbus 800, NL-9700 AV Groningen, The Netherlands;
(*vdhulst@astro.rug.nl*)

Draft version March 8, 2001

ABSTRACT

We use our recent H I and optical observations of the well known interacting system NGC 4038/9, "The Antennae", to explore the nature of the gaseous substructures found within its extensive tidal tails, including the putative tidal dwarf galaxy at the end of the southern tail. We analyze about a dozen H I concentrations within the tails, finding that they do not distinguish themselves from interclump regions in terms of their H I linewidths, optical surface brightness, or optical colors. We do find evidence that one of the star-forming regions within the tidal dwarf contains enough luminous mass to be self-gravitating, with a virial mass of $1.1\times10^8 M_\odot$, but this derivation involves significant uncertainties. The other gaseous concentrations are either not self-gravitating, or must be bound by non-luminous matter. We extend other tidal dwarf galaxy candidates reported in the literature with similar kinematic data. We find that TDG as a class do *not* contain enough luminous matter to bind them. Previous work reached the opposite conclusion by combining luminous mass indicators and dynamical linewidths in an unphysical manner. Additionally, many of the TDGs with high inferred luminous-to-dynamical masses are subject to projection effects, where tidal material piles up along the line of sight. [** What is strangely missing is a tidal dwarf candidate in a face-on tail. Best candidate remains NGC 7252. Best types of encounters for TDGs are groups rather than Toomre-Sequence like mergers. The tails in the latter are kinematically expanding, while the former can have converging gas flows. **]

Subject headings: galaxies: evolution — galaxies: individual (NGC 4038/9) — galaxies: interactions — galaxies: dwarf — galaxies: kinematics and dynamics — galaxies: peculiar

1. INTRODUCTION

Dwarf-sized condensations within tidal tails have been known about since the time of Zwicky (1956). These condensations contain many young stars (Schweizer 1978, Mirabel, Dottori, & Lutz 1992, Weilbacher et al. 2000, Saviane, Rich & Hibbard 2001) and have global properties, such as size, luminosity, H I mass, H I velocity dispersion, and CO content, in common with dwarf Irregular galaxies (Mirabel et al. 1992, Hibbard et al. 1994, Smith & Higdon 1994, Duc & Mirabel 1994, Smith & Struck 2001, Braine et al. 2000, 2001). For these reasons, such concentrations are often referred to as "Tidal Dwarf Galaxies" (hereafter TDG).

The class of Tidal Dwarfs is far from homogeneous. There is a range of structures identified as potential TDGs, ranging from detached dwarfs near interacting systems but not within any coherent tidal structure (e.g. Stephans Quintet: Mendes de Oliveira et al. 2001, Gallagher et al. 2001; NGC 5291: Malphrus et al. 1997, Duc & Mirabel 1998), to stellar systems much larger than the connecting tidal filaments (e.g. Arp 105: Duc et al. 1997; M81/NGC 3077: van der Hulst 1979, Yun, Ho & Lo 1994, Heithausen & Walter 2000; NGC 520: Stanford & Balcells 1991, Hibbard & van Gorkom 1996), to concentrations with sizes comparable to the width of the connecting tidal tail (e.g. NGC 7252: Hibbard 1994; NGC 3921: Hibbard & van Gorkom 1993,1996), to much smaller optical enhancements or star forming regions fully entrained within a tail (e.g. Hutchings 1996, Hunsberger, Charlton & Zaritsky 1996, 1998, Deeg et al. 1998, Weilbacher et al. 2000). A common presumption is that there is an evolutionary sequence between these different classes, with the small enhancements accreting surrounding material as the connecting tidal filaments fade away (e.g., Weilbacher et al. 2000, Braine et al. 2001).

Until recently, there have been few detailed studies of these objects. While this is no longer the case, kinematic studies of such structures are still rare. It has become fairly common for investigators to isolate luminous or gaseous concentrations and treat them as if they are, or will become, distinct and autonomous dynamical entities. However, strong kinematic evidence that these concentrations

[1]The National Radio Astronomy Observatory is a facility of the National Science Foundation operated under cooperative agreement by Associated Universities, Inc.

are indeed self-gravitating is lacking, and their evolution into dwarfs is therefore still in question. For some systems (e.g. M81/NGC 3077 and NGC 520/UGC 957), the supposed tidal dwarfs may be pre-existing dwarfs which have happened upon an on-going interaction and captured some tidal gas (Yun 1999, Stanford & Balcells 1991), throwing the proposed evolutionary scenario into some doubt.

It is noteworthy that this evolutionary sequence has never been explicitly demonstrated numerically. Self-gravitating models of interacting galaxies show that concentrations the size of dwarf galaxies can indeed condense within tidal tails (Barnes & Hernquist 1992; Elmegreen et al. 1993), but in the simulations the concentrations are always *sub*-structures within the tails. The bound structures collapse early, with little subsequent evolution (Barnes & Hernquist 1992), and it seems implausible on dynamical grounds that in the absence of external forces they could grow to sizes larger than the thickness of the pre-encounter disks.

The strongest cases of kinematically distinct entrained dwarfs are NGC 7252 (Hibbard 1994) and NGC 3921 (Hibbard & van Gorkom 1993, 1996). Yet the TDGs in NGC 7252 and NGC 3921 do not exhibit an unambiguous kinematic signature, such as a twisting of iso-velocity contours due to rotation around the supposed mass concentration. Instead, they show an increased H I velocity dispersion in the vicinity of the the putative tidal dwarfs. This increase has been taken as evidence of an increase in the underlying mass concentration. However, since these locations are also associated with large star forming regions, the increased linewidth could instead be due to the mechanical effects of young stars on the surrounding neutral gas (Tenorio-Tagle & Bodenheimer 1988).

NGC 4038/9 is the nearest system with an identified dwarf-galaxy sized concentration of gas, light and young stars embedded within a luminous tidal tail (Schweizer 1978). In a companion paper (Hibbard, van der Hulst, Barnes & Rich 2001, hereafter Paper I), we use high-resolution H I spectral line mapping observations and supporting ground-based optical imagery to search for the kinematic signature near the putative tidal dwarf in the southern tail of The Antennae. We find evidence for a higher velocity dispersion in this area, but the distribution of the enhanced dispersion with respect to the known star forming regions suggest that the kinematics are more likely due to star formation rather than identifying a mass concentration. The detailed examination of the TDG region presented in Paper I shows that there is something unique about this region, but whether or not it is self-gravitating is hard to ascertain.

The high-resolution H I maps of Paper I reveal a wealth of gaseous substructure within the tails of The Antennae. If tidal dwarf formation is as ubiquitous as often assumed, some of the gaseous knots should be pre-cursors to future tidal dwarfs, and should reflect this status in their kinematics and underlying stellar content. In this paper we use the H I observations to identify gaseous concentrations within the extensive tidal tails of NGC 4038/9 and to measure their gas content, velocity dispersion, and half-light radii (§2). The size and kinematics of the clumps provides a measure of the gravitational mass required for the clumps to be self-gravitating. The B-band image is used in concert with stellar population models to evaluate the possible contribution of the underlying starlight to the luminous mass. Whether or not the gaseous and stellar masses are sufficient for the clumps to be self-gravitating is then addressed (§3). Included in this analysis is a similar evaluation of the gaseous clumps found in the extensive H I tail of the Arp 299 and for the putative tidal dwarfs identified in the NGC 7252 and NGC 3921. Our results differ from recent analysis of TDGs, and in §4 we use the differences to understand the limitations and pitfalls inherent in the observations and dynamical derivations. [** Finally, in §5 we examine tidal dwarfs as a class, ... **]. Our conclusions are presented in §6.

2. GASEOUS SUBSTRUCTURE WITHIN THE TIDAL TAILS OF NGC 4038/9

The primary observations used in this paper are fully described in Paper I. They consist of high spatial and velocity resolution H I observations of NGC 4038/9 obtained with the VLA in its C and D-array configurations, and optical $B, V, \& R$ broad-band imaging from the CTIO 0.9m. In particular we use the high- and intermediate-resolution H I data, with beam dimensions (full-width at half-maximum, FWHM) of $11.4'' \times 7.4''$ and $20.7'' \times 15.4''$, respectively, and at full velocity resolution ($\Delta v = 5.2$ km s^{-1}). We also use the B-band optical image and the $B-R$ color map from Paper I.

We present the zeroth moment map of the high resolution data in greyscales in Figure 1, with a single contour from the intermediate resolution data indicating a column density of $1{\times}10^{20}\,\mathrm{cm}^{-2}$. Within this figure we outline boxes labelled I–IV, which delineate the regions shown in Fig. 2, where the high resolution H I data is contoured upon the B-band image.

In Fig. 2 we use lower-case letters $a-n$ to identify representative regions within the intermediate resolution H I datacube. Regions $j, k\&\ l$ lie in the region associated with the putative Tidal Dwarf identified by Schweizer (1978) and studied by Mirabel et al. (1992; see Paper I). The remaining regions, hereafter referred to as "clumps", were chosen to have a single channel peak that is six times the rms noise and a contrast from the surrounding gas of a factor of two or more. This threshold ensures that we measure the half-power properties of the line-profiles with a 3σ level confidence. The flux density threshold of 5.4 mJy beam^{-1} corresponds to a single channel column density limit of $1{\times}10^{20}\,\mathrm{cm}^{-2}$, or an integrated column density of $2.4{\times}10^{20}\,\mathrm{cm}^{-2}$ for a Gaussian line profile with a dispersion of 5.2 km s^{-1}. For comparison, we also evaluate the properties of an equal number of inter-clump regions, which are indicated in Fig. 2 with dashed circles and labelled with upper-case letters $A-N$.

Both the H I and optical properties of the clumps and inter-clump regions are tabulated in Tables 1 & 2. Table 1 gives the raw measured quantities, while Table 2 gives the results of fitting gaussians to the H I line profiles. In Fig. 3 we plot histograms of the H I velocity dispersion, H I column density, B-band surface brightness and $B-R$ color separately for the clump and inter-clump regions. The bottom panels show histograms for the entire southern tail, constructed from the H I moment maps and optical images. As to be expected, both the clump and interclump regions (which were chosen to lie upon the optical tail) are characterized by larger than average H I column densities. Otherwise, Fig. 3 shows that the clumps do not distinguish themselves from the inter-clump regions or from the southern tail in terms of their H I linewidths, optical surface brightness, or optical colors. For the most part, H I column density peaks do *not* have corresponding optical enhancements. The majority of the clumps are simply gas density enhancements, with no obvious indication that they are distinct entities. This is similar to what was found for the gaseous condensation within the extensive gas-rich tidal tail of the Arp 299 system (Hibbard & Yun 1999).

The line-profiles become very broad in the vicinity of clump *b* and interclump region *B*. This is not due to these tidal regions being projected onto the disk; these regions are well separated from the disk H I, and are part of the continuous linear kinematic structure of the southern tail seen in the position velocity plot shown in Fig. 3 of Paper I. This broad but single-valued structure extends all the way back to the northwestern region of the disk of NGC 4038. The broad line profiles may arise from a mix of tidal material that has reached apocenter and is streaming back towards the main disk, as well as tidal material which is still moving outward. Detailed modeling will test this hypothesis. [** tcross=22 MYR. WHAT DOES THIS TELL US? **]

In Table 2 we list the H I masses (M_{HI}), half-light radii ($r_{1/2}$), and blue luminosities (L_B) for the clump regions. Using the intermediate resolution data, the H I mass is estimated from the flux enclosed within a region slightly larger than the defining contours in Fig. 2. The B-band luminosity is calculated by summing the optical flux over the same region. The half-light radius is calculated by assuming a gaussian spatial flux distribution, with a total flux corresponding to M_{HI} and a peak flux density corresponding to the N_{HI} listed in Table 2.

3. DYNAMICAL ANALYSIS

We wish to take advantage of the higher spatial and velocity resolution of our H I observations to examine the dynamical nature of the gaseous knots lying within the tails of The Antennae, and especially those in the vicinity of the TDG. To this end, we compare the virial mass inferred from the H I linewidth (M_{vir}) to the total luminous mass inferred from the H I flux and the optical luminosity (M_{lum}). The virial mass is calculated via $\frac{GM_{vir}}{ar_{1/2}} = 3\sigma_{1D}^2$, where G is the gravitational constant, σ_{1D} is the velocity dispersion along one dimension, a is a geometric factor, equal to 2.74 for a uniform density sphere, and $r_{1/2}$ is the projected half-light radius (Binney & Tremaine 1987). This reduces to $M_{vir} = 1.91 \times 10^6 M_\odot \times \sigma_{HI}^2 \times r_{1/2}$, with σ_{HI} in km s^{-1} and $r_{1/2}$ in kpc. This quantity is tabulate for each of the clumps in column (10) of Table 2. This equation under-estimates the virial mass if material with a velocity dispersion greater than σ_{HI} contributes significantly to the luminous mass. This would be the case if evolved stellar populations from the pre-encounter disk dominate the luminous mass (e.g. van der Kruit 1988).

It is more difficult to place tight constraints on the luminous mass. There is an uncertainty due to the fact that we observe gaseous and optical flux densities that are integrated over the line of sight, which is likely to be much larger than the size of a clump[2]. A simple correction to the flux density measured at the location of a mass concentration is to subtract off the expected mass falling within the same area at a location without a suspected mass concentration; e.g. $Flux_{corr} = (\Sigma_{on} - \Sigma_{off}) \times Area$, where Σ_{on} and Σ_{off} are the surface brightnesses of the locations with and without a clump, respectively. Setting the uncorrected flux, $Flux_{raw}$, equal to $\Sigma_{on} \times Area$, we have $Flux_{corr} = Flux_{raw} \times (1 - \Sigma_{off}/\Sigma_{on})$. To place upper and lower limits on the luminous mass of the clumps, we calculate M_{lum} both with and without this off-source correction. The uncorrected H I masses and optical luminosities are given in columns (5) and (7) of Table 2, and the off-source H I column densities and optical surface brightnesses (measured just beyond the defining H I contour in Fig. 2) are given in columns (8) and (9). Note that because of they way there are selected, the ratio of the off- and on-source H I column densities are equal to one-half in almost all cases.

There is an additional uncertainty in M_{lum} due to the unknown mass-to-light ratio (M_*/L_B) of the tidal stellar population. We use the population synthesis models of Bruzual & Charlot (1999), kindly run by Bill Vacca, to bracket the acceptable range of M_*/L_B. Adopting a Salpeter IMF and Solar metallicity, we find values ranging from 2 $M_\odot\, L_\odot^{-1}$ (constant star formation history) to 5 $M_\odot\, L_\odot^{-1}$ (exponentially decreasing star formation history with a time constant of 4 Gyr) for a population with an age of 10 Gyr (values would be 20% smaller for an age of 8 Gyr). Values are also calculated with $M_*/L_B = 0$ (i.e., stars contribute negligibly to the luminous mass) to place a firm lower limit to the luminous mass in the vicinity of the clumps.

The last step is to derive a gas mass from the observed H I mass. This is done by multiplying the H I mass by a factor of 1.36 to take into account a primordial abundance of Helium. No correction is made for the presence of molecular gas. Recent CO observations at the location of the TDG by Gao et al. (2001) and Braine et al. (2001) find only trace amounts of molecular gas ($4 \times 10^6 M_\odot$), so this approximation is likely valid.

The final equation for M_{lum} may then be written

$$\begin{aligned} M_{lum} &= 1.36 \times M_{HI} \times [1 - N_{HI,off}/N_{HI,on}] \\ &+ (M_*/L_B) \times L_B \times [1 - 10^{0.4(\mu_{on} - \mu_{off})}] \quad (1) \end{aligned}$$

The relevant H I and optical masses, column densities, luminosities and surface brightnesses are all listed in Tables 1 & 2.

In Figure 4 we plot M_{lum}/M_{vir} for each clump, calculating M_{lum} both with (filled symbols) and without (empty symbols) the off-source correction, and for stellar mass-to-light ratios of 0 $M_\odot\, L_\odot^{-1}$ (upward pointing triangles), 2 $M_\odot\, L_\odot^{-1}$ (squares) and 5 $M_\odot\, L_\odot^{-1}$ (downward pointing triangles). We also indicate the expected values of M_{lum}/M_{vir} for bound ($M_{lum}/M_{vir} > 0.5$, dotted line) and virialized ($M_{lum}/M_{vir} = 1$, dashed line) regions. We connect all points, except those calculated with the highest M_*/L_B values; this is because those values involve an

[2]Taking the mean observed velocity dispersion of 7 km s^{-1} (Fig. 3) and the approximate time since the tails were launched of 420 Myr (Paper I), we infer a minimum tail width of 3 kpc, which is much larger than any of the half-light radii tabulated in Table 2

inconsistency — the high M_*/L_B is appropriate for a uniformly old population, and such populations have much higher velocity dispersions than the gas (e.g. van der Kruit 1988), in which case M_{vir} is underestimated. So we consider these points to be firm upper limits to M_{lum}/M_{vir} rather than reasonably obtainable values.

Figure 4 shows that most of the clumps in NGC 4038/9 are unbound for all of the reasonable values of M_{lum} that we evaluate. Three regions stand out for their high M_{lum}/M_{vir} ratios: regions $g, i, \&l$. The first two of the regions have low values of M_{lum}/M_{vir} when only the gas is considered, but because they are quite extended and of high optical surface brightness, they obtain quite large values when the starlight and the higher M_*/L_B values are adopted. Given the uncertainty in the stellar mass determinations, it is not possible to say whether these regions are indeed self-gravitating, but they may be. Region l, on the other hand, is almost bound even considering the minimum value for M_{lum} (gas only, including off-source correction). Therefore we believe it is likely that region l is self-gravitating.

For the remainder of the clumps, many of the upper limits lie in the "bound" region ($M_{lum}/M_{vir} > 0.5$). However, given the small sizes of the clumps and the large expected width of the tail, we suspect that the lower values of M_{lum}/M_{vir} (i.e., those calculated including the off-source correction) are more realistic. Further, the fact that these gaseous concentrations do not have optical counterparts suggests that stars do not contribute significantly to their luminous mass. These results suggest that the majority of the clumps are not self-gravitating, but are simply gas density enhancements. Conversely, if the clumps *are* self-gravitating, Fig. 4 suggests that their gravitational mass must be dominated by non-luminous matter.

[** ANYTHING ABOUT CROSSING TIMES? RANGE FROM 60–120 Myr, EXCEPT b, WHICH IS 20 Myr **]

To the right in Fig. 4 we plot M_{lum}/M_{vir} for the tidal dwarf in the tail of The Antennae (from Paper I; labelled N4038S) and from similar regions found within the tidal tails of NGC 7252 (from Hibbard et al. 1994), NGC 3921 (from Hibbard & van Gorkom 1993, 1996) and Arp 299 (from Hibbard & Yun 1999). For NGC 7252 and NGC 3921 we plot only the regions identified with putative tidal dwarf galaxies: one in each tail of NGC 7252 (labelled N7252W and N7252E in Fig. 4), and one in the southern tail of NGC 3921 (labelled N3921S). There are no TDGs identified within the optically faint, gas-rich tidal tail of Arp 299, and the values plotted in Fig. 4 represent the highest values found for the gaseous peaks. The values of M_{lum}/M_{vir} found for NGC 7252E and Arp 299 are low, supporting the conclusions reached in Hibbard et al. (1994) and Hibbard & Yun (1999) that these regions are not self-gravitating. The values for NGC 7252N and NGC 3921S are similar to those found for the TDG region in NGC 4038/9, and these regions may be, but need not be, self-gravitating. Further studies are needed to more tightly constrain this ratio; in particular, measurements of the stellar velocity dispersion and a better constraint on the stellar mass-to-light ratio.

[** I AM NOT MARRIED TO THE IDEA OF INCLUDING THIS PARAGRAPH: **] A possible evolutionary scenario is suggested by the fact that clumps j and k have a higher velocity dispersion than region l, and as a result a lower value of M_{lum}/M_{vir}, and by noticing that the gas velocity dispersion is increased in the vicinity of the star forming regions (Fig. 6d of Paper I). This suggests that some clumps may have been self-gravitating, but when they started to form stars the resulting energy input due to the winds of young stars and supernovae increases the kinetic energy of the clump sufficiently to unbind them. Only a few regions (less than or of order 1 per tail) have sufficient mass to remain bound in spite of the increased energy due to star formation.

4. COMPARISON WITH OTHER WORK

In a recent paper, Braine et al. (2001) reported on CO spectral observations of TDGs. Their dynamical analysis led them to conclude that tidal dwarfs do indeed have enough luminous matter to be self-gravitating. We examine this result in a bit more detail here, since their conclusion relied heavily on a correlation between the dynamical and luminous mass, with most of the correlation given by the TDGs in NGC 4038 and NGC 7252W. Our evaluation of the dynamical and luminous mass of these two systems do not agree with theirs, so it is of interest to understand why this is so.

Braine et al. plot the dynamical mass estimator $M_{dyn} = G^{-1}R\Delta V^2$ vs. various indicators of the luminous mass. The dynamical mass reduces to the equation for M_{vir} given in §3 when ΔV is taken to be FWHM linewidth (equal to $2.35\sigma_{1D}$ for gaussian lines) and R is set equal to $2r_{1/2}$. They find a correlation between the dynamical mass and the various baryonic mass indicators, arguing that the correlation suggests that the TDGs are self-gravitating. Further, they find that many of the systems lie close to or below the $M_{dyn} = M_{gas}$ line, concluding that there is enough mass in gass alone for these regions to be self-gravitating.

In Figure 5 we reproduce the four correlations used in Braine et al. (2001, Fig. 10) [** ACTUALLY, I REALLY ONLY USE THE MGAS AND MGAS+2LB VS MDYN PANELS, SO PERHAPS I DON'T NEED TO SHOW ALL FOUR. BOTH 4-PANEL AND 2-PANEL VERSIONS ARE ON THE WEBPAGE **] . In particular, we plot M_{dyn} against the molecular mass inferred from the CO flux M_{mol}, the total gas mass[3] inferred from both H I and CO observations M_{gas}, the blue luminosity L_B, and the quantity $M_{gas} + 2L_B$ as an indication of the total stellar plus gaseous mass. The data evaluated by Braine et al. are plotted as filled triangles. Data evaluated in this paper are plotted as small crosses (gas clumps the the tails of NGC 4038/9) and open triangles (TDGs in NGC 4038S, NGC 7252W, NGC 7252E, NGC 3921S). The values for NGC 4038S and NGC 7252W used by Braine et al. are connected to the values adopted in this study by dotted lines. A solid line in each panel indicates when M_{dyn} is equal to the quantity it is plotted against, and systems lying below and to the right of this line have enough mass to account for the observed linewidth.

Figure 5 shows that the points that we adopt for NGC 4038Sand NGC 7252W are very different from those use

[3]Are value differs from that plotted by Braine et al. 2001 in that we include a factor of 1.36 to account for the contribution of Helium to the total gas mass.

by Braine et al. (2001). This can be traced to two factors: Firstly, the $r_{1/2}$ used in our analysis is based on the spatial distribution of the H I gas, whereas R in the Braine et al. analysis is derived from the size of the beam of their CO observations. Taking into account that $2r_{1/2} = R$ for $M_{vir} = M_{dyn}$, this results in a difference by a factor of 4–5. Secondly, Braine et al. evaluate the dynamical mass by adopting linewidths measured from single-dish measurements of the CO(1-0) or CO(2-1) spectra lines, whereas we use the H I linewidths, and the former are narrower than the latter by factors of 3–4. These combined effects lead to a total difference in the dynamical mass estimates of factors of 30–60.

The stellar and H I contributions to the luminous mass should only be compared to the dynamical mass inferred from the CO linewidth if the H I and stellar light are in fact distributed like the CO. The fact that the CO linewidths are several times narrower than the H I linewidths proves that the H I at least is not distributed like the CO. The broader H I linewidths indicate either that the H I traces a larger potential than the CO, or is more affected by kinetic agitation by tidal motions and/or star formation. Eitherway, the kinetic energy per unit mass for the H I is larger than for the molecular gas, and requires a larger mass to bind it than inferred from the CO linewidth. Similarily, the stellar mass should not be added to the luminous mass unless there is good reason to believe that the stellar light has a similarly low velocity dispersion. This might be true of a burst population, but in such a case a low mass-to-light ratio should be used to calculate the stellar mass. Using the H I mass, stellar light with a high mass-to-light ratio, and the CO linewidth to evaluate the dynamical and luminous masses is unphysical and inconsistent.

Clearly, the fact that there are molecular gas concentrations and on-going starformation indicates that material is bound on *some* scale. The CO linewidth likely reflects this scale. It just has not yet been shown what this scale is, and whether it is large enough for the forming systems to be long-lived dynamical entities.

It is interesting that there is a clear correlation between the dynamical mass and the luminous mass indicators. Braine et al. interpret this as further evidence that the TDG candidates are self-gravitating. However, the correlation is Fig. 5d is offset by 0.7 dex from the $M_{lum} = M_{dyn}$ line, so the relationship does not prove that TDGs are self-gravitating. *If* the candidates *are* self-gravitating, it says that 80% of their mass has a high mass-to-light ratio (or is dark). Some of the TDG considered by Braine et al. do lie quite close to the $M_{dyn} = M_{lum}$ line (specifically NGC 4676, Arp 245, Arp 105, and NGC 7319E), but as discussed in the next section we believe there are problems with the mass and dynamical estimates of these systems due to projection effects.

In short, we conclude that some regions within tidal tails may be self-gravitating, but that the evidence is far from conclusive. The main lesson we learn from this exercise is that it is important to use consistent quantities when evaluating the dynamical mass.

5. ARE ANY TIDAL DWARFS SELF-GRAVITATING?

[** I HAVE SKETCHED OUT SOME IDEAS. IS THIS WORTH DEVELOPING? **]

We restricted the analysis of the previous section to data that we directly have access to for making the measurements. In this section, we consider other systems referred to in the literature as being TDG candidates and examine if there is undeniable evidence that such systems form and are self-gravitating. We restrict this investigation to systems which have kinematic information available, so we do not address the giant H II regions or light concentrations reported by e.g. Hunsberger et al. (1996), Weilbacher et al. (2000).

The definition of TDG that we consider here is... JOSH, WOULD YOU DARE GIVE A DEFN? self-gravitating system should have the following attributes: crossing time much shorter than dynamical time,.. Mtidal vs Mcomplexes? Does this give us a minimum mass? $r_{tidal} \sim r_{dwarf} \times (m/M)^{1/3}$ This is a restricted defn of TDG; we do not consider systems that form from tidally torn material – systems referred to as "Recycled Galaxies" by Duc. There are many ways for tidal gas to re-assemble (shocks, converging flows, 3-body encounters). Here we consider structures forming on their own within expanding tidal debris, independent of exterior forces. Other recycled galaxies may be more common and may even be more important that the formation mechanism we are concentration on. But their inclusion will confuse matters when trying to establish under what conditions concentrations form within tidal tails. [** I MAY BE SPLITTING HAIRS WITH THIS SEPARATION OF TDG CLASSES**]

NGC 7252W: only system w/symmetric distribution of gas, starlight, star formation, increase in H I linewidth. Recent HST observations find 5 SSCs within the TDG, whereas none are found elsewhere along the tail (Kniermann et al. 2001). The age of the SSCs inferred from their location in the color-magnitude is a few 10 Myr, which is much less than the dynamical age of the tails. Strong circumstantial evidence that this is a local potential in this region. Still, not definitive - need to ascertain that increased line-width is not due to star formation. If bound, mass greater than tidal mass and should be long lived companion to NGC 7252 remnant (HM95).

NGC 7252E: kinematics not ordered, so not as good of a candidate. Two SSCs found by Kniermann et al. (2001).

NGC 3921: Similar to NGC 7252, but kinematic signature less distinct. Needs more study. No SSCs.

Compact group candidates (eg SQ, HCG 31): many candidates, but nor much kinematic information (notable exception is Stephans Quintent, refs). Dynamically different than what we are concentrating on, b/c the multiple potentials make the dynamics much more complicated: allows for tidally ejected gas to follow converging streamlines. Also gas may shock where ICM is colliding (eg., regions 1-5 & 6 in SQ). So while these might become separate entities, their formation mechanism is different from concentrations condensing and growing within tidal debris. Interesting case is galaxy 8 in SQ, which is within a tail, has distinct kinematics, well-behaved and symmetric rotation curve. Very high DM ratio. Not clear how this could form from a DM poor tail.

Related to the compact group candidates are those found in group environments. Example is gaseous concentrations near NGC 3077 in the M81 system: high H I column density, sizable molecular concentration that should have recently condensed, but near existing dwarf galaxy — allows for converging gas flows. So not strictly what we are talking about. Probably related system is UGC 966 near NGC 520 (Arp 157).

NGC 5291: a strange system, but not clear what the hell it is. Optical tails very ratty, no clear progenitor. Fact that dwarfs lie off of the metallicity-magnitude relationship for dwarfs means that they are good candidates for being recycled, but it is not clear that they were generated whole cloth from tidally expanding material, a la BH92 or EKT.

Finally, there are an uncomfortable number of systems which appear at the ends of gaseous tails exactly where we expect these features to be bending away from us along the line-of-sight. In such cases the gas, emission line and light concentrations may arise from the increased pathlength along the line-of-sight, and the kinematics may reflect geometric effects rather than the presence of a local mass concentration. Candidates here are Arp 105, Arp 245 (NGC 2992/3), NGC 4676, and IC 1182. We note that three of these had the highest luminous-to-dynamical mass ratios in Fig. 5 (Arp 105, Arp 245, NGC 4676), so we find these datapoints to be highly suspect. Arp 105N has the added problem that it is so much more extended than the tail and has a crossing time which is much longer than the age of the tail. While this may indeed be a recycled dwarf, we find it kinematically implausible that it formed as a mass concentration within the thin tidal tail.

Apparent superpositions: Superantennae (Duc, personal communication), many clumps in SQ.

Observations do suggest that some self-gravitating regions appear in tidal tails (with NGC 7252W being the best candidate). In agreement with numerical simulations, these candidates have sizes smaller than the width of the tidal tail, so it is dynamically plausible that they formed in the manner seen in numerical simulations. Need to find best candidates so we can determine under what conditions they form, how ubiquitous, how many, how long lived, dark matter dominated or not, possibly related to dSph and halo building.

We differentiate these from the systems Duc has called Recycled Dwarfs — dwarfs formed from material that was previously within another system. And this material has likely been thrown out by tidal interactions. Best evidence is the distinct kinematics as traced by Hα rotation curves and the high metallicity for their absolute magnitude. Prime candidates are N5291, SQ. Important as recently assembled systems, but confusing when trying to figure out when dwarfs form in tails.

Note that the recycled galaxies may be more important to the formation of dwarfs in a cosmological context. At high redshift, group encounters should be more common than Toomre-like enconters. Possibility of converging flows may lead to higher efficiency of tidal gas assembling into distinct systems. Also, long-tailed Toomre-like mergers necessarily have largest tidal shear, which should limit the size of any concentrations, which may further decrease efficiency of TDG formation.

Somewhere should we note that the Elmegreen mechanism is not likely to be playing a role in such features? Observations prove that tails are dynamically cold, with mean dispersion similar to that observed in pre-encounter disks.

6. CONCLUSIONS

- We characterize the properties of many H I density enhancements within the tidal features. We find that the majority of the clumps do not distinguish themselves from interclump regions in terms of their H I linewidths, optical surface brightness, or optical colors. There does not appear to be enough luminous material present for these condensations to be self-gravitating. We conclude that the majority of the clumps are not self-gravitating, and are simply gas density enhancements, with no obvious indication that they are distinct kinematic entities. We do find evidence that one region is self-gravitating: the region identified as star forming region III by Mirabel et al. (1992) and labelled region l in our study,

- The putative Tidal Dwarf Galaxies found in the tails of NGC 4038/9, NGC 3921, and NGC 7252 may or may not be self-gravitating. For all systems evaluated, we find that they need both stellar mass and some dark matter to bind. Further insight requires a measurement of the stellar velocity dispersion and tighter constraints on the stellar mass-to-light ratio.

- The determination of a virial or dynamical mass requires some care. Have to use values self-consistently. Can't use CO line-width and H I mass. CO linewidth likely reflects dynamics on a much smaller scale.

- Many of the best-studied tidal dwarfs candidates are found in tails that are bending away from us along the line-of-sight. In such cases the gas, emission line and light concentrations may arise from the increases pathlength along the line-of-sight, and the kinematics may reflect geometric effects rather than the presence of a local mass concentration. What would be really convincing would be a face-on candidate or candidate mid-way along a tidal tail, where projection effects would not play a role. Best case for kinematically distinct TDG forming within a tidal tail remains NGC 7252.

- Toomre sequence mergers may not be best environoment for TDG formation. Large kinematic gradients. Better environment may be group environment, where you can have converging gas flows.

JEH would like to thank the participants of the Saclay meeting on Tidal Dwarf Galaxies, particularly Pierre-Alaine Duc, Jonathan Braine, Vassilis Charmandaris, Francois Combes, Peter Weilbacher, Ute Liesenfield, Nathalie, Chantal, Polis ... . for a lively and enriching discussion.

Bill Vacca for running population synthesis models for us.

REFERENCES

Barnes, J. E., & Hernquist, L. 1992, Nature, 360, 715
Binney, J., & Tremaine S. 1987, "Galactic Dynamics", (Princeton: Princeton University Press).
**Braine, J., Duc, P.-A., Lisenfeld, U., Leon, S., Vallejo, O., Charmandaris, V. & Brinks, E. 2001, A&A, submitted
Braine, J., Lisenfeld, U., Duc, P.-A., & Leon, S., 2000, Nature, 403, 867
Bruzual, A. G. & Charlot, S. 1993, ApJ, 405, 538
Duc, P. -A 1995, Ph. D. Thesis, Université Paris
***Duc, P. -A., Brinks, E., Springel, V., Pichardo, B., Weilbacher, P., & Mirabel, I.F., 2000, AJ, ***, ***
Duc, P. -A., Brinks, E., Wink, J. E., & Mirabel, I. F. 1997, A&A, 326, 537
Duc, P. -A., Mirabel, I. F. 1994, A&A, 289, 83
Duc, P. -A., Mirabel, I. F. 1998, A&A, 333, 813
Elmegreen, B., Kaufmann, M., & Thomasson, M. 1993, ApJ, 412, 90
Gao, Y., Lo, K. Y., Lee, S.-W., & Lee, T.-H. 2001, ApJ, 548, 172
**Gallagher, S. C., Charlton, J. C., Hunsberger, S. D., Zaritsky, D., & Whitmore, B. C. 2001, AJ, submitted
Heithausen, A., & Walter, F. 2000, A&A, 361, 500
**Hibbard, J. E., van der Hulst, J. M., Barnes, J. E., & Rich, R.M.R 2001, AJ, submitted
Hibbard, J. E., & van Gorkom, J. H. 1996, AJ, 111, 655
Hibbard, J. E., & van Gorkom, J. H. 1993, in ASP conf. series, Vol. 48, The Globular Cluster–Galaxy Connection, eds. G. H. Smith and J. P. Brodie (ASP, San Francisco), 619
Hibbard, J. E., Guhathakurta, P., van Gorkom, J. H., & Schweizer, F. 1994, AJ, 107, 67
Hibbard, J.E., & Mihos, J.C. 1995, AJ, 110, 140.
Hibbard, J. E., & Yun, M. S. 1999, AJ, 118, 162
Hunsberger, S., Charlton, J., & Zaritsky, D. 1996, ApJ, 462, 50
Hunsberger, S., Charlton, J., & Zaritsky, D. 1998, ApJ, 505, 536
Hutchings, J. B. 1996, AJ, 111, 712
***Knierman, K. A., Gallagher, S. C., Charlton, J. C., Hunsberger, S. D., Whitmore, B., Kundu, A., Hibbard, J. E., & Zaritsky, D. 2001, AJ, in press
Malphrus, B. K., Simpson, C. E., Gottesman, S. T. & Hawarden, T. G. 1997, AJ, 114, 1427
**Mendes de Oliveira, C., Plana, H., Amram, P., Balkowski, C., & Bolte, M., 2001, AJ, in press
Mirabel, I. F., Dottori, H., & Lutz, D. 1992, A&A, 256, L19
***Saviane, I., Rich, R.M.R., & Hibbard, J.E. 2001, in preparation
Schweizer, F. 1978, "The Structure and Properties of Nearby Galaxies", IAU Symp. No. 77, edited by E. M. Berkhuijsen and R. Wielebinski (Reidel, Dordrecht), p. 279
Smith, B. J., & Higdon, J. L. 1994, AJ, 108, 837
**Smith, B. J., & Struck, C. 2001, ApJ, submitted
Stanford, S. A., & Balcells, M. 1991, ApJ, 370, 118
Tenorio-Tagle, G., Bodenheimer, P. 1988, ARA&A, 26, 145
van der Hulst, J. M. 1979, A&A, 75, 97
van der Kruit, P. C. 1988, A&A, 192, 117
Weilbacher, P. M., Duc, P.-A., Fritze-v.Alvensleben, U., Martin, P., & Fricke, K. J. 2000, A&A, 358, 819
Yun, M. S. 1999, in IAU Symp/. No. 186, Galaxy Interactions at Low and High Redshfit, ed. D. Sanders & J. Barnes (City: Publisher) 81
Yun, M. S., Ho, P. T. P., & Lo, K. Y. 1994, Nature, 372, 530
Zwicky, F. 1956, *Ergebnisse der Exakten Naturwissenschaften*, 29, 344

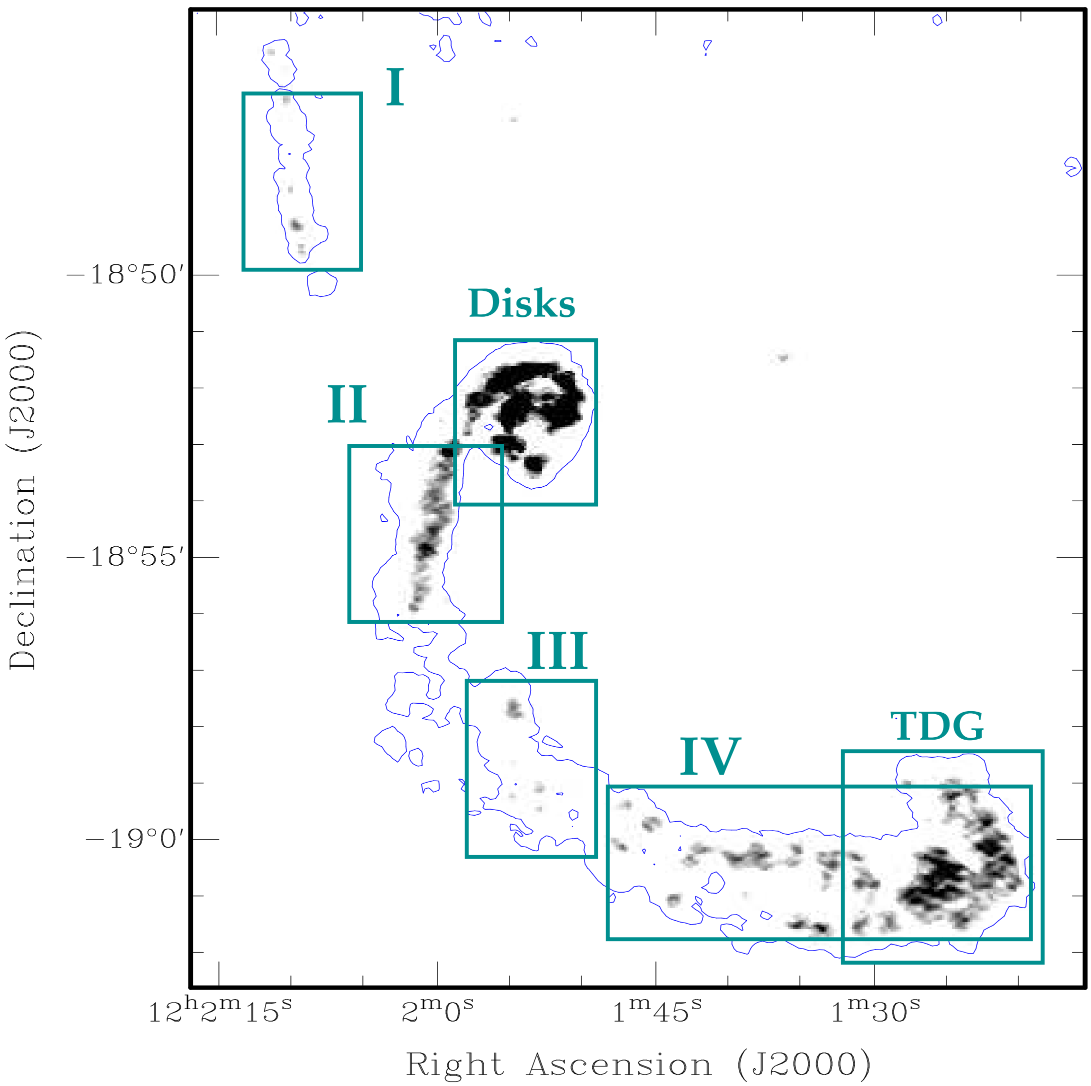

FIG. 1.— A greyscale representation of the integrated H I emission from the high resolution datacube, with a single contour from the intermediate resolution drawn at a column density of $1{\times}10^{20}\,\mathrm{cm}^{-2}$. The boxes labelled I–IV delineate the regions shown in Fig. 2.

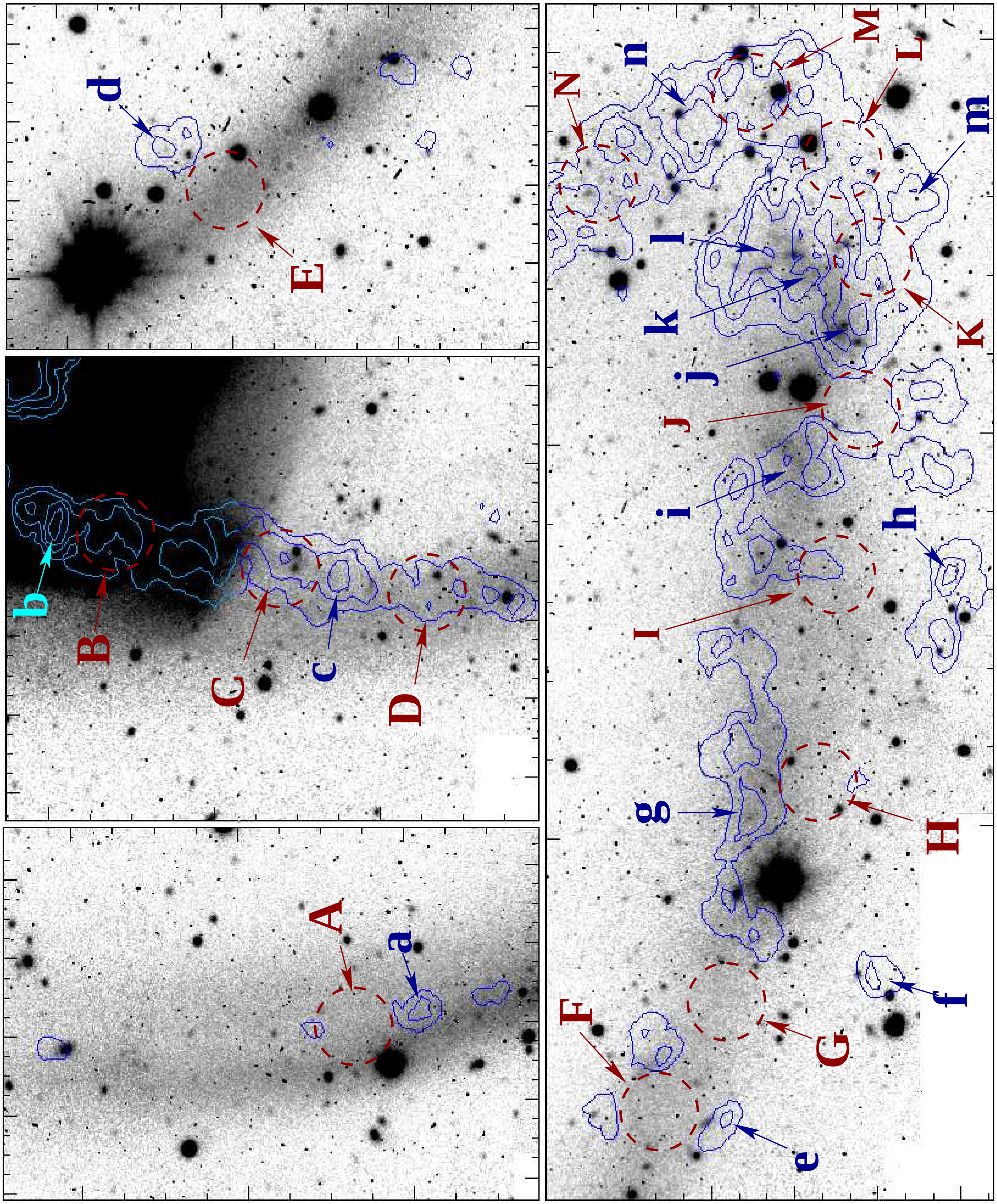

FIG. 2.— A close-up of the regions labelled I—IV in Fig. 1. The high resolution H I data is shown contoured upon a greyscale representation of the optical B-band image. The H I contours are drawn at levels of (1.5, 5.0, 10.0, 15.0) $\times 10^{20}$ cm^{-2}. Representative H I density enhancements are labelled $a-n$, while inter-clump regions are indicated with dashed circles and labelled $A-M$. The properties of these regions are tabulated in Tables 1 & 2.

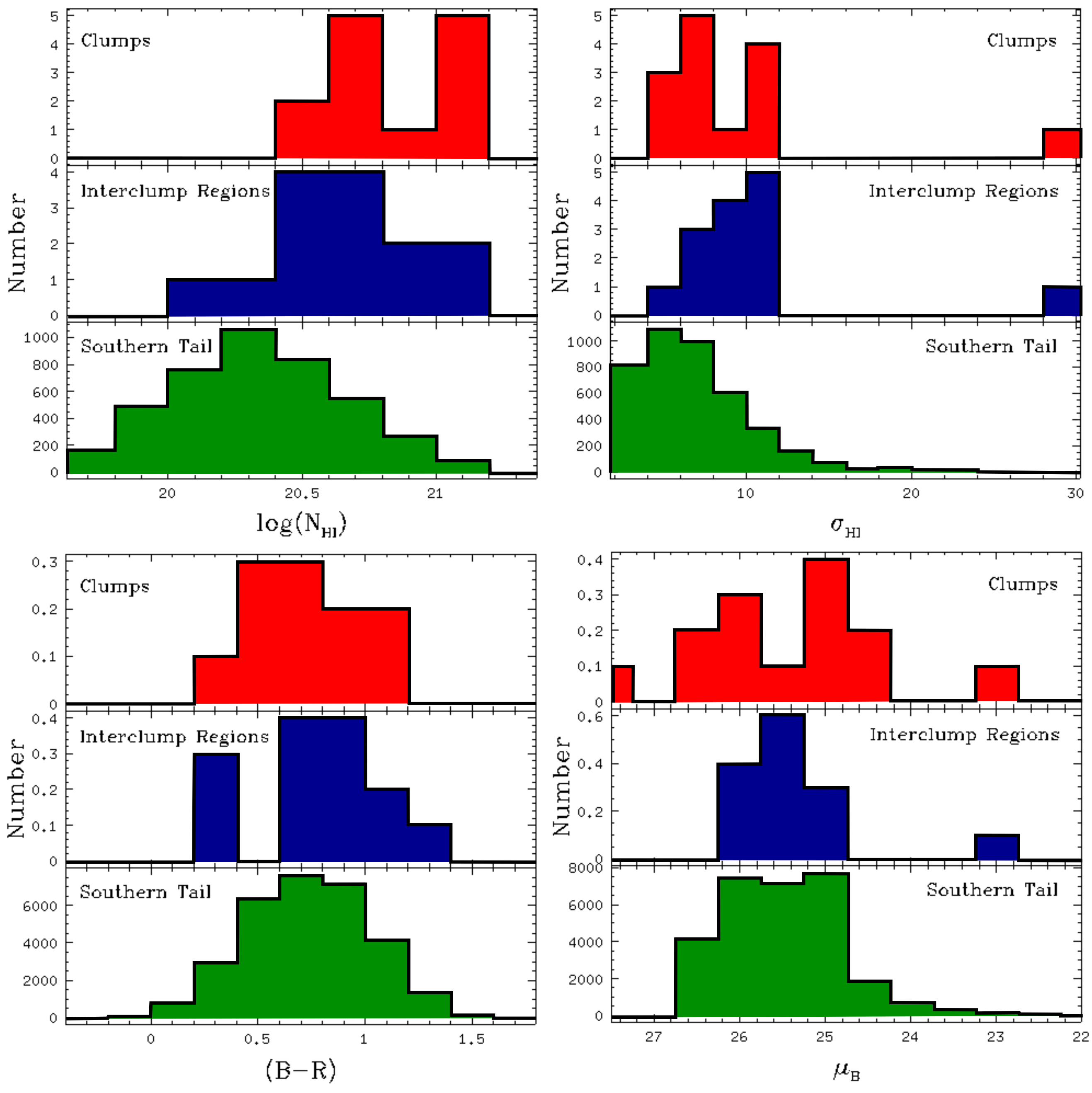

FIG. 3.— Histograms of H I and optical properties for the clumps identified in Fig. 2 (top panel), interclump regions (middle panel), and entire southern tail (bottom panel). The properties compared are (a) the logarithm of the H I column density (measured from the zeroth moment map for the bottom panel); (b) H I velocity dispersion (measured from the second moment map for the bottom panel); (c) B-band surface brightness; and (d) $B - R$ colors.

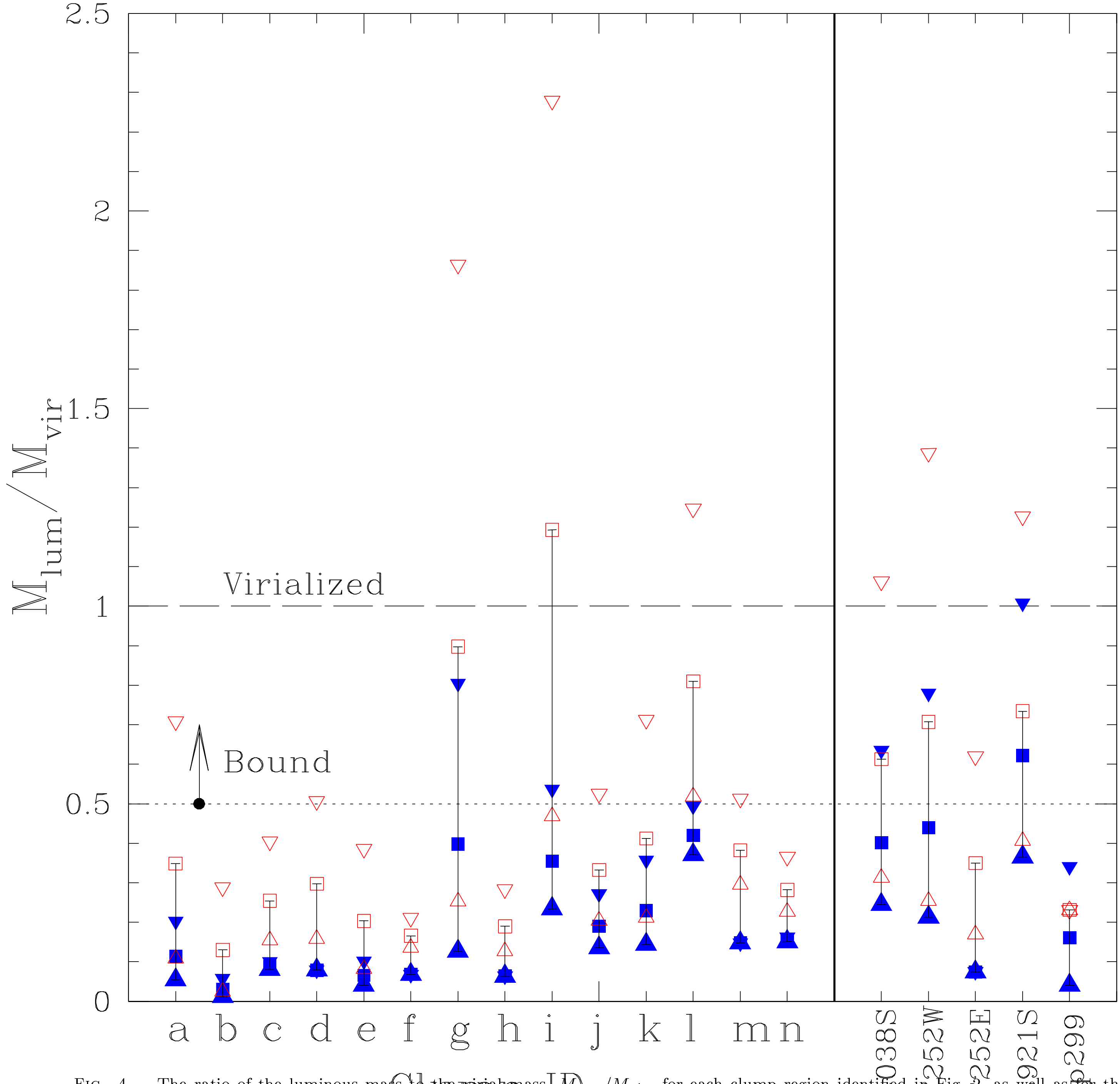

Fig. 4.— The ratio of the luminous mass to the virial mass, M_{lum}/M_{vir}, for each clump region identified in Fig. 2, as well as for the region of the tidal dwarf as a whole (labelled "TDG"). To the right we indicate values obtained for gaseous clumps within tidal tails of other systems: NGC 7252 (putative TDGs in the north and east tail, labelled "N7252N" and "N7252E", from Hibbard et al. 1994), NGC 3921 (putative TDG in the southern tail, labelled "N3921S", from Hibbard & van Gorkom 1993, 1996), and Arp 299 (numerous gaseous knots but no TDG, from Hibbard & Yun 1999a). The plotted symbols represent different values of M_{lum}. Filled symbols include an off-source correction to account for material along the line-of-sight which is not within the vicinity of the the clump, whereas empty symbols have no off-source correction, and will be firm upper limits. Different symbols are used for different values for the stellar mass-to-light ratio, ranging from 0 $M_\odot\, L_\odot^{-1}$ (upward pointing triangles), 2 $M_\odot\, L_\odot^{-1}$ (squares) and 5 $M_\odot\, L_\odot^{-1}$ (downward pointing triangles). Values that fall above the dotted line at $M_{lum}/M_{vir} = 0.5$ indicate bound regions, while values larger than the dashed line at $M_{lum}/M_{vir} = 1$ will be virialized. See §3 for details.

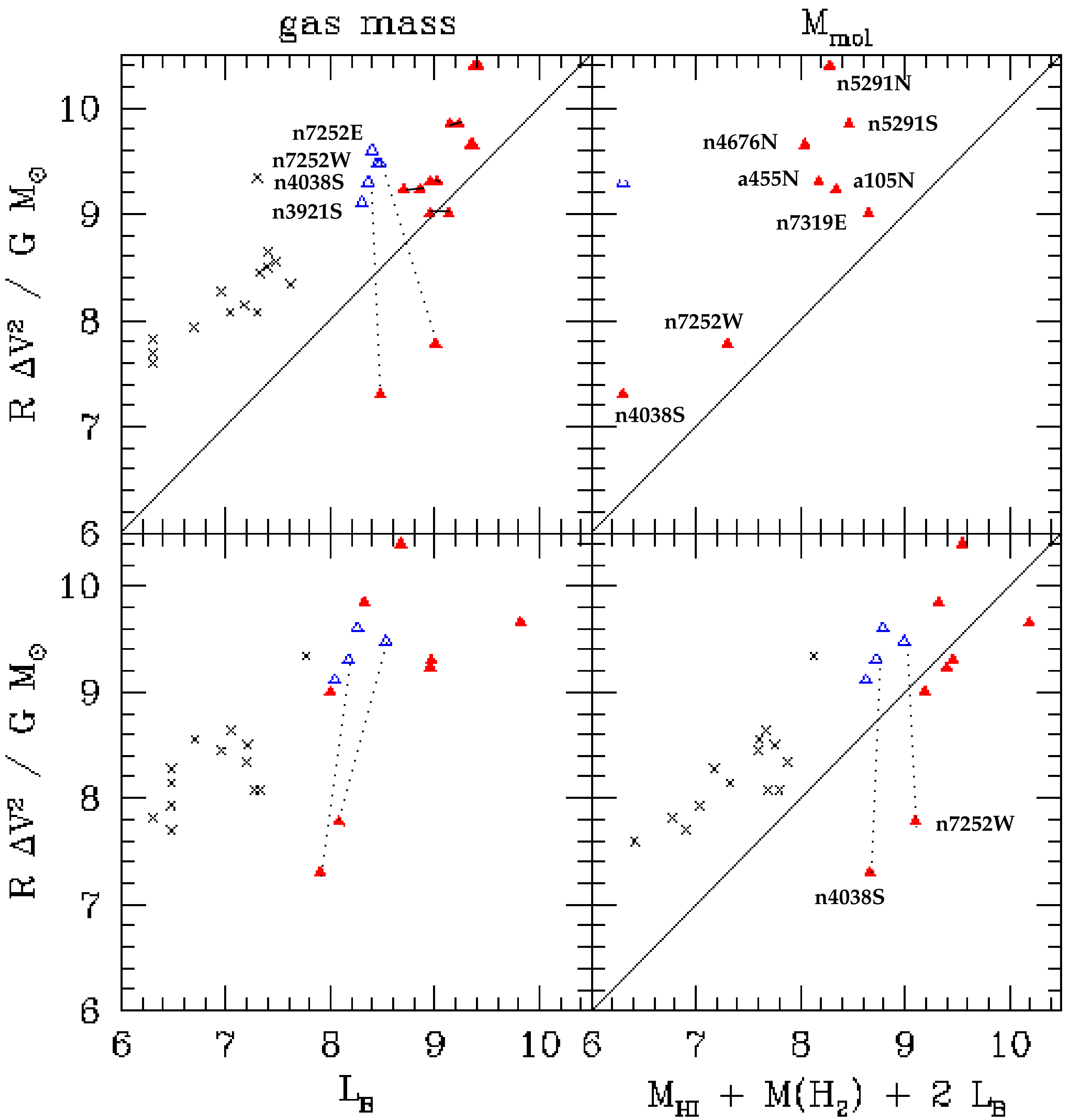

FIG. 5.— Dynamical mass indicator, $\Delta V^2 R/GM_{\odot}$, vs. the gas mass $M_{gas} = (M_{HI} + M_{H2}) \times 1.36$ and the luminous mass indicator $M_{gas} + 2L_B$, showing our points and Braines. Describe. ALSO TAKE A LOOK AT 2-PANEL VERSION ON WEBPAGE

Table 1
Measured Properties of Regions in Tails of NGC 4038/9

(1) Region	(2) R.A. (J2000)	(3) Dec. (J2000)	(4) Distance (kpc)	(5) $V_\odot$ (km s^{-1})	(6) $\Delta V_{\rm HI}$ (km s^{-1})	(7) S_{HI} (mJy b^{-1})	(8) $\mu_{B,on}$ (mag/ □″)	(9) $\mu_{B,off}$ (mag/ □″)	(10) $B-R$ (mag)
Gas Clumps:									
a	12 02 09.7	–18 49 04	29.3	1578	–52	7.4	25.1	25.4	1.20±0.04
b	12 01 59.2	–18 53 06	7.9	1607	–15	6.4	23.0	23.2	1.09±0.04
c	12 02 00.7	–18 54 48	15.4	1681	+52	10.0	25.3	25.4	0.89±0.04
d	12 01 54.8	–18 57 37	28.4	1736	+104	7.7	26.0	26.0	0.97±0.04
e	12 01 47.2	–19 00 06	43.3	1765	+136	7.0	25.8	26.0	0.67±0.04
f	12 01 43.8	–19 01 00	49.1	1759	+130	8.0	27.4	27.0	—
g	12 01 39.5	–19 00 18	47.1	1756	+125	8.7	24.7	25.3	0.67±0.04
h	12 01 33.6	–19 01 33	57.4	1737	+110	8.4	26.4	26.4	—
i	12 01 30.9	–19 00 45	55.3	1738	+110	10.8	25.0	25.3	0.66±0.04
j†	12 01 27.0	–19 01 02	58.8	1723	+94	15.6	25.1	25.7	0.42±0.04
k	12 01 26.0	–19 00 42	58.9	1719	+89	15.9	24.7	25.3	0.45±0.04
l†	12 01 25.2	–19 00 31	58.1	1710	+78	21.0	25.0	25.3	0.50±0.04
m	12 01 24.0	–19 01 23	62.3	1710	+78	11.7	26.7	26.7	—
n	12 01 22.0	–19 00 07	59.6	1664	+32	14.2	26.1	26.2	0.30±0.04
Inter-clump Regions:									
A	12 02 10.1	–18 48 25	31.6	1774	–54	5.8	25.4	—	1.27±0.04
B	12 01 59.2	–18 53 25	8.4	1624	–8	6.0	23.2	—	1.09±0.04
C	12 02 00.3	–18 54 25	13.2	1668	+40	9.8	24.8	—	0.88±0.04
D	12 02 01.0	–18 55 25	18.3	1693	+64	5.4	25.1	—	1.08±0.04
E	12 01 56.4	–18 57 55	30.0	1743	+112	4.6	25.0	—	0.90±0.04
F	12 01 46.9	–18 59 45	41.0	1761	+130	2.1	25.4	—	0.69±0.04
G	12 01 44.1	–19 00 05	43.8	1764	+132	3.6	25.5	—	0.90±0.04
H	12 01 38.8	–19 00 40	49.4	1757	+130	3.7	25.4	—	0.95±0.04
I	12 01 33.5	–19 00 50	53.4	1746	+115	6.9	25.3	—	0.77±0.04
J	12 01 29.6	–19 01 05	57.3	1737	+105	6.3	25.8	—	0.72±0.04
K	12 01 25.4	–19 01 10	61.0	1715	+84	8.4	26.2	—	0.30±0.04
L	12 01 22.9	–19 01 00	62.4	1698	+68	7.4	26.2	—	0.65±0.04
M	12 01 21.2	–19 00 25	61.5	1671	+41	12.0	25.8	—	0.39±0.04
N	12 01 23.3	–18 59 35	56.3	1652	+22	7.5	25.5	—	0.22±0.04

(1) Region of measurement, as labelled in Fig. 2.

(4) Projected radial distance of region from center of NGC 4038/9 for an adopted a distance of 19.2 Mpc.

(5) Heliocentric velocity of H I.

(6) Line-of-sight velocity of H I relative to the systemic velocity of 1630 km s^{-1}.

(7) Measured H I flux density peak, from intermediate resolution data at the full velocity resolution of 5.21 km s^{-1}.

(8) B-band surface brightness

(9) For clumps only, the off-clump surface brightness, used to calculate correction for line-of-sight integration effects. See §3 for details.

(10) $B-R$ color with 1σ errors. These are only calculated for regions which have a signal-to-noise greater than five in both the B- and R-band images.

† Location of star forming regions identified by Mirabel et al. 1992.

Table 2
Derived Properties of Regions in Tails of NGC 4038/9

(1) Region	(2) $S_{HI,fit}$ (mJy b^{-1})	(3) σ_{HI} (km s^{-1})	(4) $N_{HI,on}$ (cm^{-2})	(5) $N_{HI,off}$ (cm^{-2})	(6) M_{HI} ($M_\odot$)	(7) $r_{1/2}$ (kpc)	(8) L_B ($L_\odot$)	(9) M_{vir} ($M_\odot$)	(10) t_{cross} (Myr
Gas Clumps:									
a	6.7	5.7	3.3×10^{20}	1.7×10^{20}	2.0×10^{6}	0.41	3.0×10^{6}	2.5×10^{7}	72
b	4.9	29.5	1.3×10^{21}	6.7×10^{20}	2.0×10^{7}	0.65	5.8×10^{7}	1.1×10^{9}	22
c	9.7	11.8	9.9×10^{20}	4.9×10^{20}	2.5×10^{7}	0.84	1.1×10^{7}	2.3×10^{8}	71
d	7.8	6.3	4.2×10^{20}	2.1×10^{20}	5.0×10^{6}	0.57	3.0×10^{6}	4.3×10^{7}	90
e	6.5	6.7	3.7×10^{20}	1.9×10^{20}	2.0×10^{6}	0.39	2.0×10^{6}	3.4×10^{7}	58
f	7.8	5.2	3.6×10^{20}	1.8×10^{20}	2.0×10^{6}	0.39	3.0×10^{5}	2.1×10^{7}	75
g	8.3	6.1	4.4×10^{20}	2.2×10^{20}	1.1×10^{7}	0.83	1.9×10^{7}	5.9×10^{7}	136
h	7.2	8.6	5.4×10^{20}	2.7×10^{20}	9.0×10^{6}	0.68	3.0×10^{6}	9.7×10^{7}	79
i	10.6	5.4	5.0×10^{20}	2.5×10^{20}	2.0×10^{7}	1.05	2.1×10^{7}	5.9×10^{7}	194
j†	13.9	10.1	1.2×10^{21}	6.0×10^{20}	2.1×10^{7}	0.70	9.0×10^{6}	1.4×10^{8}	69
k	13.3	10.5	1.2×10^{21}	6.0×10^{20}	2.5×10^{7}	0.76	1.6×10^{7}	1.6×10^{8}	72
l†	20.0	7.8	1.4×10^{21}	6.0×10^{20}	4.2×10^{7}	0.91	1.6×10^{7}	1.1×10^{8}	117
m	11.6	6.8	6.8×10^{20}	3.4×10^{20}	1.5×10^{7}	0.78	3.0×10^{6}	6.8×10^{7}	115
n	13.2	10.6	1.2×10^{21}	6.0×10^{20}	3.0×10^{7}	0.83	5.0×10^{6}	1.7×10^{8}	78
Inter-clump Regions:									
A	4.9	8.4	3.6×10^{20}						
B	4.6	28.3	1.1×10^{21}						
C	8.9	9.7	7.5×10^{20}						
D	4.6	11.4	4.6×10^{20}						
E	4.7	8.6	3.5×10^{20}						
F	2.3	7.7	1.5×10^{20}						
G	4.0	6.0	2.1×10^{20}						
H	3.4	11.7	3.4×10^{20}						
I	6.5	4.7	2.7×10^{20}						
J	4.7	10.6	4.3×10^{20}						
K	8.2	10.4	7.4×10^{20}						
L	8.1	7.0	4.9×10^{20}						
M	12.1	9.6	1.0×10^{21}						
N	7.3	10.0	6.3×10^{20}						

$^{(1)}$Region of measurement, as labelled in Fig. 2

$^{(2)-(4)}$Peak H I flux ($S_{HI,fit}$) and H I velocity dispersion (σ_{HI}) derived from Gaussian fits to the line profiles, and the corresponding peak H I column density ($N_{HI,on}$).

$^{(5)}$Off-clump column density, used to calculate correction for line-of-sight integration effects. See §3 for details.

$^{(6)-(8)}$For clump regions only: H I mass (M_{HI}), half-light radius ($r_{1/2}$), and B-band luminosity without any correction for line-of-sight integration effects, calculated as described in §2.

$^{(9)}$Virial Mass, calculated via $M_{vir} = 1.91\times10^{6} M_\odot \times \sigma_{HI}^2 \times r_{1/2}$. See §3 for details.

$^{(10)}$Crossing-time, calculated via $t_{cross} = r_{1/2}/\sigma_{HI}$.

†Locations nearest the star forming regions identified by Mirabel et al. 1992.